

Electrocleavage Synthesis of Solution-Processed, Imine-Linked, and Crystalline Covalent Organic Framework Thin Films

Lingling Wang,^{II} Changwen Xu,^{II} Weiqi Zhang, Qinglei Zhang, Manlin Zhao, Cheng Zeng, Qinglin Jiang, Cheng Gu,* and Yuguang Ma*



Cite This: *J. Am. Chem. Soc.* 2022, 144, 8961–8968



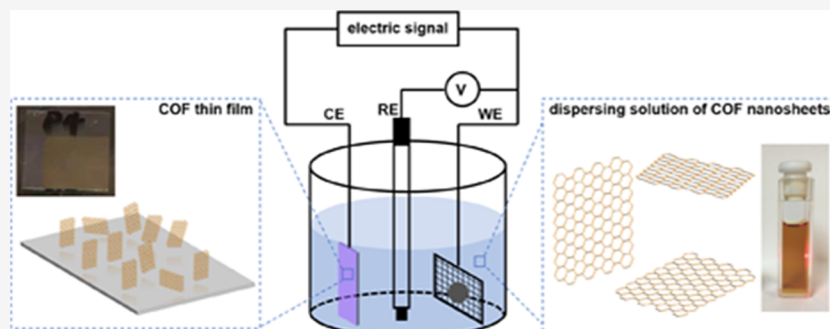
Read Online

ACCESS |

Metrics & More

Article Recommendations

Supporting Information



ABSTRACT: Developing a general, facile, and direct strategy for synthesizing thin films of covalent organic frameworks (COFs) is a major challenge in this field. Herein, we report an unprecedented electrocleavage synthesis strategy to produce imine-linked COF films directly on electrodes from electrolyte solutions at room temperature. This strategy enables the cathodic exfoliation of the COF powders to nanosheets by electrochemical reduction and protonation, followed by nanosheets migrating to the anode and reproducing the COF structures by anodic oxidation. Our method is adaptable with most imine-linked COFs by virtue of the low redox potential of the imine bonds, whereas the COF films possess high crystallinity and hierarchical porosity. We highlight these COF films as a superb platform for promoting mass transfer by demonstrating their extraordinarily rapid iodine adsorption with record-high rate constants.

INTRODUCTION

Covalent organic frameworks (COFs), in which molecular building blocks are covalently organized into periodic structures, have attracted extensive attention for their low density, high stability, and tailored functionalities.^{1–3} COFs have shown promising potential in applications such as separation,⁴ energy storage and conversion,⁵ and catalysis.⁶ However, COFs are inherently crosslinked and are usually produced as insoluble and isolated microcrystalline powders, which impede many membrane-/film-based applications. Recently, significant efforts have been made in the preparation of COF nanosheets, thin films, and membranes, toward the processing of COFs for expanding their application aspects.⁷ Currently, two main approaches, namely bottom-up^{8–11} and top-down^{12,13} strategies, have been developed. Despite the significant progress in the COF film preparation, drawbacks including low crystallinity for the bottom-up strategy and limited crystal domains for the top-down strategy still exist.⁷ Banerjee's group¹⁴ and our group¹⁵ developed self-exfoliated COFs bearing ionic frameworks, which are highly dispersible in organic solvents to form large-area COF sheets and can be readily prepared into high-quality membranes. Nevertheless, this strategy is only limited to a few COFs. To develop a

general strategy for facile synthesis of a large variety of COF films remains challenging but would constitute a major achievement in this field.

Electrochemical redox thin-film deposition has proven to be a useful technology for preparing electroactive semiconducting polymer films directly on electrodes without involving auxiliary deposition processes.¹⁶ This method can readily introduce plenty of charge/radical species into the polymer skeletons accompanied by the insertion of counterions in the redox process. Therefore, this strategy is feasible for COF film deposition triggered by redox sweeping to regulate the dispersibility of COFs in electrolyte solutions. Herein, we report an unprecedented, general, and facile electrocleavage synthesis strategy at room temperature to convert imine-linked two-dimensional (2D) COFs from unprocessable powders to

Received: December 13, 2021

Published: April 5, 2022



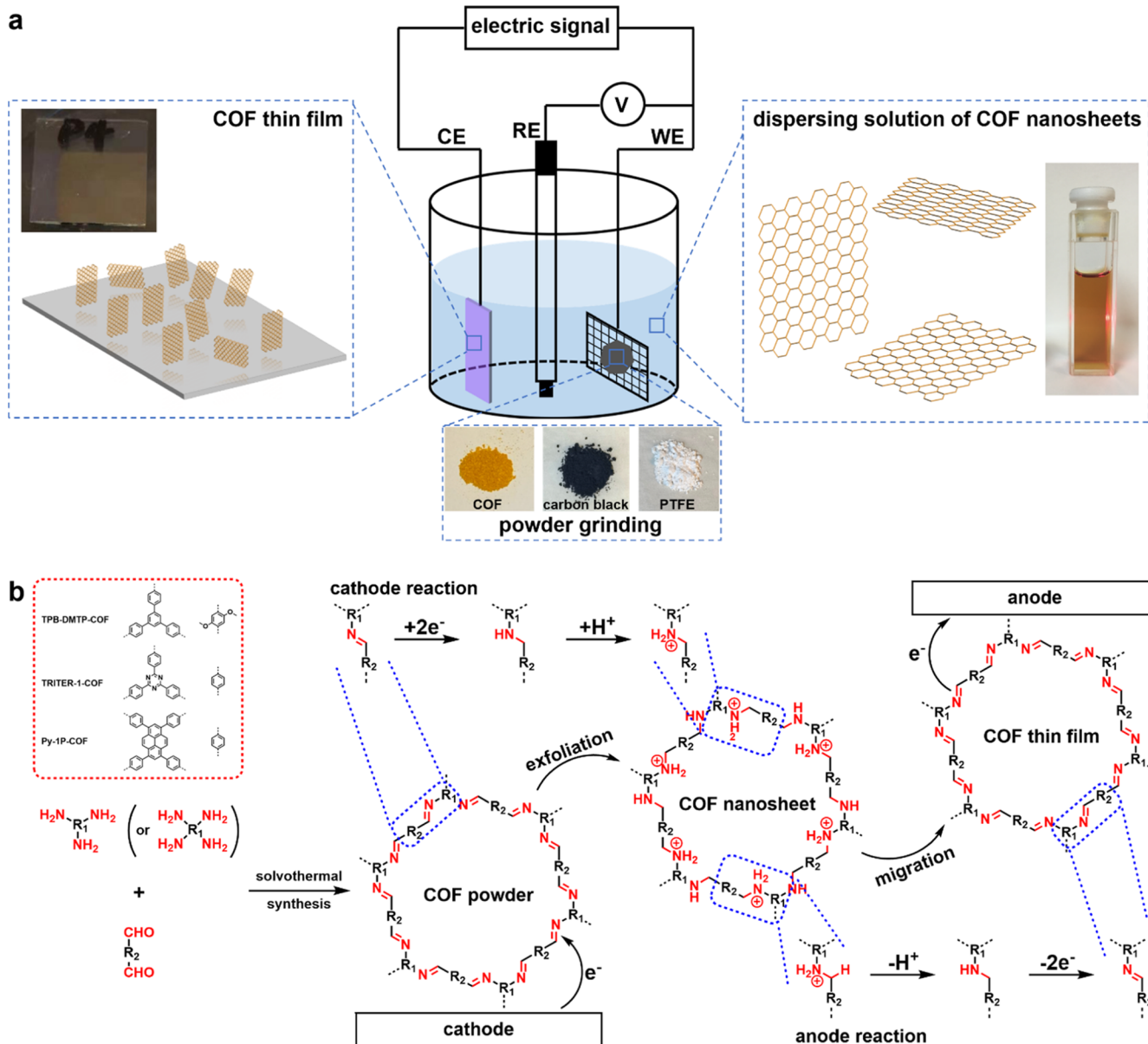


Figure 1. (a) Depicting the rationale of the electrocleavage synthesis strategy to produce COF films. The cathodic reduction produces protonated amine COF nanosheets, which migrate to the counter electrodes and undergo anodic oxidation to yield crystalline COFs as thin films on the electrodes. (b) Total electrode reactions in the electrocleavage synthesis process.

thin films (Figure 1a). This method takes advantage of cathodic reduction to transfer the imine bonds to the protonated amine bonds and introduces plenty of positive charges to the COF skeletons, thereby exfoliating COFs to large-area nanosheets that are highly dispersible in the electrolyte solutions (Figure 1b). Subsequently, these COF nanosheets migrate to the counter electrodes driven by the electric fields and undergo anodic oxidation to recover the imine bonds from the protonated amine bonds and reproduce crystalline COFs as thin films on the electrodes (Figure 1b). One important feature is that the reductive onset potential of the imine bonds is from -0.4 to -0.9 V, which is distinguishable from that of the COF building blocks. Therefore, this method possesses substantial universality to most imine-linked COFs without decomposing their chemical structures, giving rise to large-area COF nanosheets with high dispersibility. This makes a sharp contrast to traditional

mechanical exfoliation that only yields nanosheets with very limited areas. Additionally, this approach is rapid and is operated under mild conditions, thus opening a new pathway for processing high-quality COF films. We highlight the utility of these COF films in iodine adsorption with exceptionally rapid uptake kinetics.

RESULTS AND DISCUSSION

Electrochemical Exfoliation from COF Powders to Nanosheets. We chose three classic COFs, namely TPB-DMTP-COF,¹⁷ TRITER-1-COF,¹⁸ and Py-1P-COF,¹⁹ with different chemical and crystal structures, as examples to illustrate the generality of our strategy (Figure 1b). The three COFs were synthesized according to the literature (Supporting Information, Figure S1), and their chemical structures and crystallinities were undisputedly confirmed by Fourier-transform infrared (FT-IR) spectra (Supporting

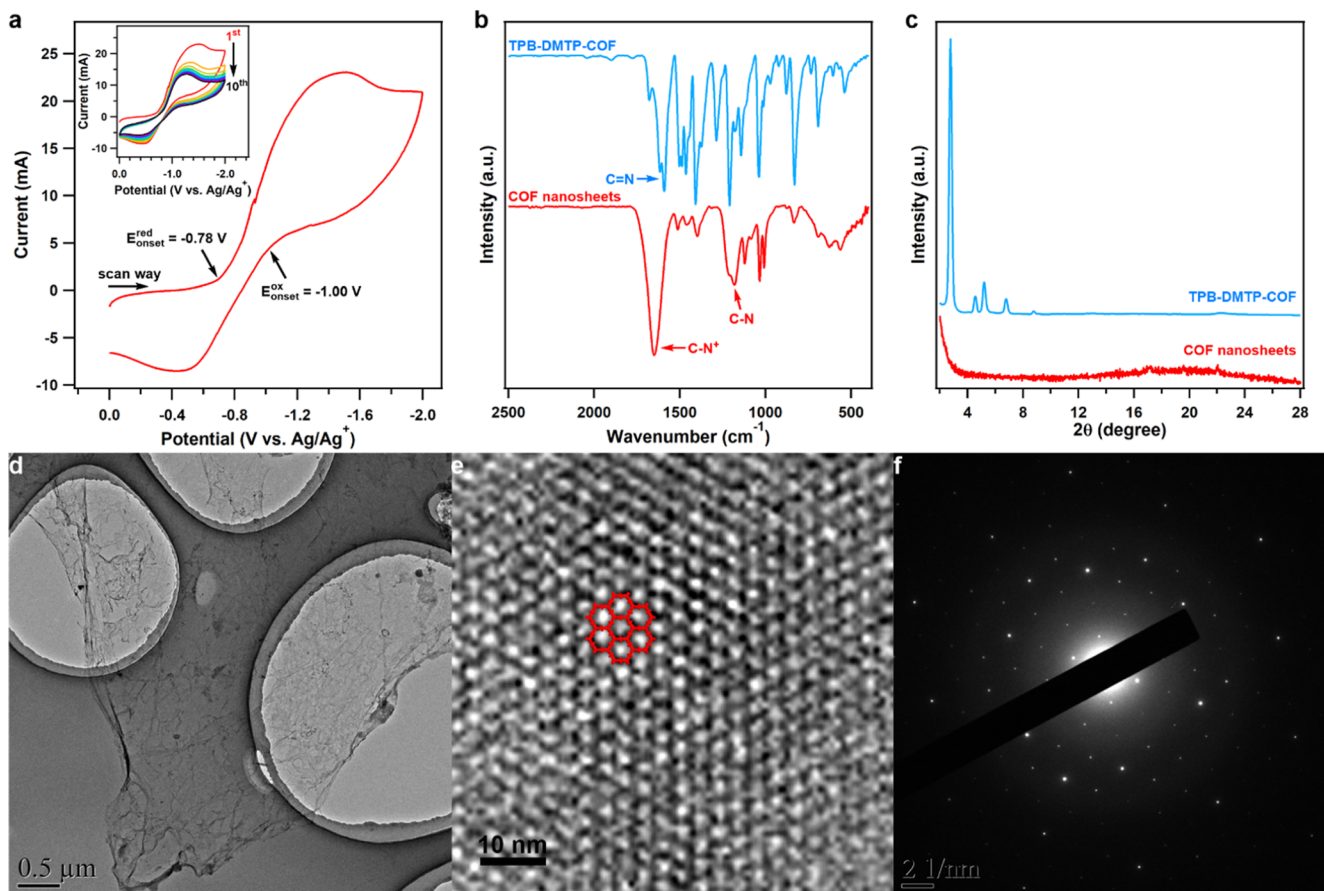


Figure 2. (a) CV profile (first cycle) of TPB-DMTP-COF in DMF containing 0.1 M LiClO₄ and 0.01 M PTSA with a scan rate of 0.05 V s⁻¹ on the Pt mesh. TPB-DMTP-COF was mixed with carbon black and PTFE by grinding. The inset is the 1st to 10th cycles showing the current decrease with the scan cycles. (b) FT-IR spectra of TPB-DMTP-COF powder and electrochemically exfoliated nanosheets. (c) PXRD patterns of TPB-DMTP-COF powder and electrochemically exfoliated nanosheets. (d) TEM image of a TPB-DMTP-COF nanosheet at low magnification, showing the large area of several micrometers. (e) TEM image of a TPB-DMTP-COF nanosheet at high magnification, showing the hexagonal pores. (f) SAED pattern of a TPB-DMTP-COF nanosheet, revealing high crystallinity.

Information, Figure S2) and powder X-ray diffraction (PXRD) (Supporting Information, Figure S3). Subsequently, the electrocleavage synthesis of COF films was performed in a three-electrode electrochemical cell containing *N,N*-dimethylformamide (DMF) as an electrolyte solution, 0.1 M lithium perchlorate (LiClO₄) as a supporting electrolyte, and 0.01 M *p*-toluenesulfonic acid (PTSA) as a proton source (Figure 1a, Supporting Information, Figure S4). Taking TPB-DMTP-COF as an example, it was mixed with conductive carbon black (Super P Li) and polytetrafluoroethylene (PTFE) to grind into a sheet, which was then pasted on a platinum mesh to serve as the working electrode. Indium tin oxide was employed as the counter electrode, and the Ag/Ag⁺ was used as the reference electrode. The electrocleavage synthesis was monitored by cyclic voltammetry (CV) in the potential range from 0 to -2.0 V. From the first cycle of the negative scan, the onset potential at -0.78 V accounted for the reduction of the imine bonds with the formation of amine bonds (Figure 2a), followed by protonation by PTSA to generate protonated amine bonds. This process introduced a large number of positive charges to the COF skeletons and exfoliated the COF powders into nanosheets by electric repulsion.²⁰ The charged nanosheets were highly dispersible in the electrolyte solution, which made the color of the electrolyte solution change from colorless to light orange, as could be directly visualized by naked eyes. On

the subsequent positive scan, oxidation with an onset potential of -1.0 V and a peak potential of -0.5 V was observed, which could be assigned to the oxidation of the positively charged amine bonds generated in the former scan to obtain neutral imine bonds. From the second cycle on, both anodic and cathodic currents constantly decreased with the number of cycles (Figure 2a, inset), illustrating that the product was dispersed in the electrolyte solution gradually with the cycle number. After 10 cycles, the color of the electrolyte solution turned orange-brown, whereas a clear yellow-color, continuous, and compact film was generated on the ITO counter electrode (Figure 1a, Supporting Information, Figure S7a). Similar phenomena were also observed in the cases of TRITER-1-COF and Py-1P-COF (Supporting Information, Figures S5 and S6), yielding yellow and light-orange films (Supporting Information, Figure S7b,c).

We first characterized the COF nanosheets dispersed in the electrolyte solutions. Still taking TPB-DMTP-COF as an example, constant-voltage electrolysis was performed at a negative potential of -1.0 V for 1 h (Supporting Information, Figure S8). The electrolyte solution gradually turned from colorless to brown-yellow with prolonged reaction time, indicating that the reductive and exfoliated TPB-DMTP-COF nanosheets were well generated. The rate of the reductive reaction was gradually slowed down and nearly reached

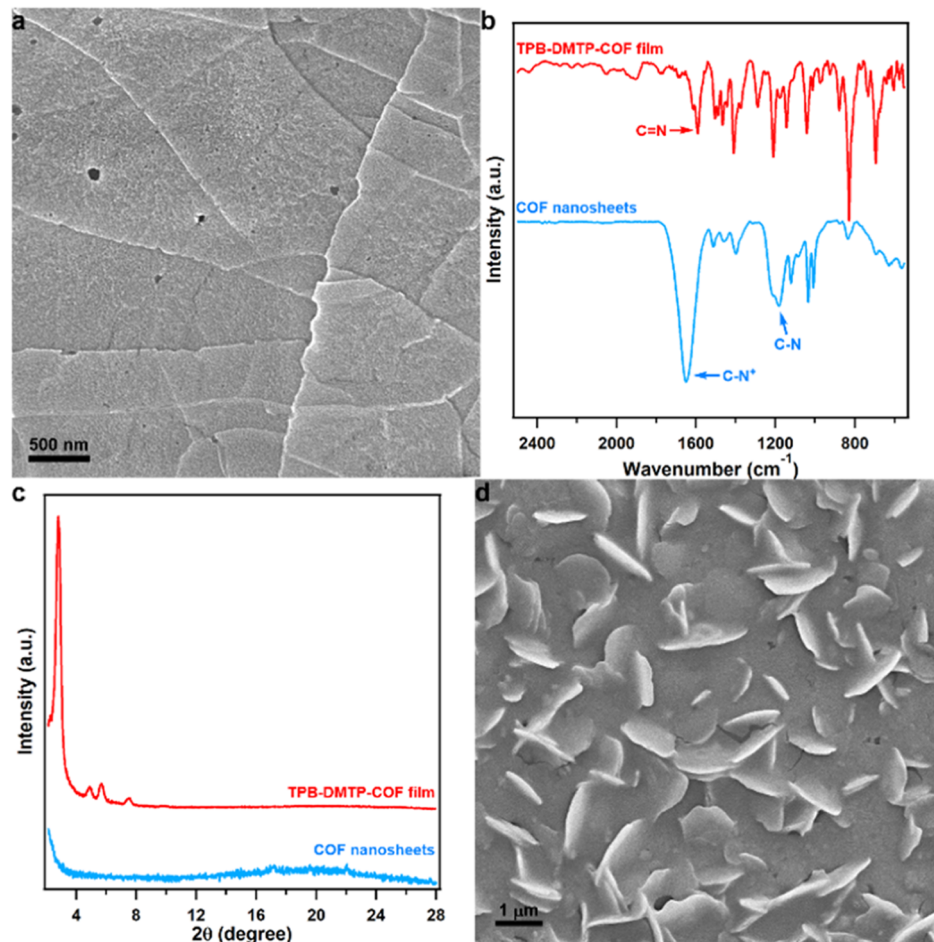


Figure 3. (a) SEM image of a drop-casted TPB-DMTP-COF nanosheet film. (b) FT-IR spectra of the TPB-DMTP-COF nanosheets and anode-deposited film. (c) PXRD patterns of the TPB-DMTP-COF nanosheets and anode-deposited film. (d) SEM image of an anode-deposited TPB-DMTP-COF thin film.

equilibrium after 30 min, as could also be indicated from the UV-vis spectra monitored at a certain interval ([Supporting Information](#), Figure S9). The nanosheets of TRITER-1-COF and Py-1P-COF could also be readily prepared by this protocol ([Supporting Information](#), Figures S10–S13). To obtain pure COF nanosheet solids, we first filtered the solution to remove any residual carbon black powder and then added acetonitrile to the DMF solution to deposit the nanosheets as a precipitate, which was further isolated by centrifugation and vacuum drying to yield powders without the residual DMF in the nanosheet samples ([Supporting Information](#), Figure S14). FT-IR spectra of TPB-DMTP-COF nanosheets showed that the peak attributing to the imine bonds at 1618 cm^{-1} disappeared after electrochemical reduction, whereas new absorption peaks belonging to C–N bonds at 1183 and 1215 cm^{-1} and the peak from C–N⁺ bonds at 1651 cm^{-1} were observed ([Figure 2b, Supporting Information](#), Table S1), indicating that the imine bonds in the TPB-DMTP-COF were successfully converted into neutral and protonated amine bonds. Notably, other peaks belonging to the two building blocks remained unchanged, which demonstrated that this method precluded the possibility of framework decomposition in the electrocleavage process. Similar phenomena were also observed in the cases of TRITER-1-COF and Py-1P-COF ([Supporting Information](#), Figure S15). PXRD of the nanosheets revealed that it completely lost the crystallinity after delamination ([Figure 2c, Supporting Information](#), Figure S16), indicative of random stacking of the nanosheets which could minimize the interlayer electrostatic repulsion. As expected, the N₂-sorption experiments at 77 K revealed negligible porosity ([Supporting Information](#), Figure S17), which was due to the random stacking in the COF nanosheet solids that blocked the nanopores for gas diffusion.

The COF nanosheets after purification could re-disperse in DMF and form transparent colloidal solutions with an obvious Tyndall effect ([Figure 1a, Supporting Information](#), Figure S18). Their morphologies were directly visualized by transmission electron microscopy (TEM). Taking TPB-DMTP-COF as an example, the initial COF powder showed a tightly stacked thick-layer structure ([Supporting Information](#), Figure S19). By contrast, the COF nanosheets after electrochemical delamination exhibited a thin-layer structure without the observation of aggregation ([Figure 2d](#)), which clearly demonstrated the successful production of highly exfoliated, ultrathin 2D COF nanosheets. Similarly, TRITER-1-COF and Py-1P-COF also showed a fully exfoliated thin-layer morphology ([Supporting Information](#), Figures S20 and S21). Notably, the size of the nanosheets reached as large as several micrometers, in contrast to the traditional mechanical exfoliation that yields the COF nanosheets with sizes less than 500 nm.²¹ High-magnification TEM revealed the ordered hexagonal pores for TPB-DMTP-COF ([Figure 2e](#)), which

directly demonstrated the intactness of the framework upon delamination. The selected area electron diffraction (SEAD) pattern showed a highly ordered arrangement with independent diffraction points (Figure 2f), which could only be observed in the case of highly crystalline materials, thus further confirming the high intralayer crystallinity of the COF nanosheets. Atomic force microscopy (AFM) of the nanosheets revealed that their thicknesses were 3–4 nm, approximately 8–10 layers (Supporting Information, Figure S22). Large-area AFM measurements also indicated that the size distribution of the nanosheets of TPB-DMTP-COF, TRITER-1-COF, and Py-1P-COF was ~10, ~5, and ~8 μm , respectively (Supporting Information, Figure S23), in sharp contrast to traditional mechanical exfoliation that only yielded nanosheets with very limited sizes.

The dispersibility of the TPB-DMTP-COF nanosheets was evaluated by measuring the UV-vis spectra in the solution combined with calibrating the molar absorption coefficient of the building blocks (Supporting Information, Figure S24–S26). Accordingly, the dispersibility of the TPB-DMTP-COF, TRITER-1-COF, and Py-1P-COF nanosheets in DMF was calculated to be 9.5, 13.3, and 13.6 mg mL^{-1} , respectively (Supporting Information, Table S2). Notably, these COF nanosheet dispersions are completely transparent, solution-like, and exceptionally stable without any sediment even left under ambient conditions for several months. These unique features make a sharp contrast to traditional COF suspensions, which are non-transparent and quickly precipitate, thus impeding the scale-up production of COF films.

Amorphous Nanosheet Films and Crystalline COF Films. Such outstanding solubility and stability of our COF nanosheets are extremely desirable for the solution preparation of COF films. We could directly prepare the COF nanosheet-based thin films by drop-casting the nanosheet dispersing solutions onto insulating or conductive substrates, followed by thermal evaporation of the solvents to afford the uniform and continuous thin films. Scanning electron microscopy (SEM) images revealed continuous films composed of nanosheets, which stacked horizontally to the substrates (Figure 3a, Supporting Information, Figure S27). Therefore, high-quality COF nanosheet thin films could be readily prepared by this facile method, which could promote the fabrication and performance screening for their optoelectronic devices.

Besides the COF nanosheets that dispersed in the electrolyte solutions, in the electrocleavage synthesis process, considerable COF nanosheets migrated to the counter electrodes driven by the electric fields and then underwent electrochemical oxidation on the neutral and protonated amine bonds to recover the imine bonds. This made the COF nanosheets re-stack because of the interlayer $\pi-\pi$ interactions.²² To confirm the nanosheet migration process, we employed an H-shape electrochemical cell equipped with an anion-exchange membrane between the working and counter electrodes to block the migration of nanosheets (Supporting Information, Figure S28). In this case, no film could be generated on the counter electrode, demonstrating that the nanosheet migration was key to achieving film deposition on the counter electrode. We conducted structural characterization of the films on the counter electrodes. FT-IR spectra of the thin films revealed a regenerated peak at 1593 cm^{-1} , attributed to the imine bonds, along with the disappearance of the peaks at 1183, 1215, and 1651 cm^{-1} , which belong to the C–N and C–N⁺ bonds (Figure 3b, Supporting Information, Figure S29). Additionally,

no over oxidation in the other parts of the structures was observed, as could be recognized from the constant peak positions with the initial COF powders. X-ray photoelectron spectroscopy (XPS) measurements for the thin films exhibited almost consistent profiles with those of their powders, which further indicated the reformation of imine bonds (Supporting Information, Figures S30–S32, Table S3). These results clearly confirmed the complete recovery of the chemical structures of imine-linked 2D polymers after electrochemical oxidation. PXRD patterns of the films revealed clear peaks with positions identical to those of the initial COF powders (Figure 3c, Supporting Information, Figure S33), which indicated that the crystallinity of the COF films was also recovered from the nanosheets. This could be easily understood from the strong $\pi-\pi$ interactions among the neutral, imine-linked COF layers after the electrochemical oxidation. The full width at half maximum (FWHM) of the dominant PXRD peaks for the films of TPB-DMTP-COF, TRITER-1-COF, and Py-1P-COF was 0.42, 0.72, and 0.20°, respectively, whereas they were 0.16, 0.81, and 0.17° for powder samples, respectively. Accordingly, the average crystalline domain sizes in the films of TPB-DMTP-COF, TRITER-1-COF, and Py-1P-COF were 118, 69, and 267 nm, respectively, whereas they were 309, 61, and 290 nm in their powders, respectively. N₂-sorption curves at 77 K revealed an almost recovered porosity compared with the initial COF powders, whereas a characteristic steep increase in the uptake capacity was observed at a high pressure of $0.8 < P/P_0 < 1$ (Supporting Information, Figures S34 and S35), which corresponded to the condensation of N₂ on the macropores of the COF film surfaces by the capillarity effect, thus demonstrating the existence of hierarchical porosity in the COF films.

Interestingly, SEM images of the COF films revealed that the COF nanosheets were separately deposited on ITO electrodes with homogeneous dispersion (Figure 3d, Supporting Information, Figures S36 and S37), thereby showing a hierarchical porosity. This could be ascribed as a kinetic-controlled deposition process, in which the COF nanosheets upon the electrochemical oxidation rapidly stacked and deposited on the ITO electrodes, in contrast with the drop-casted film-forming process, where considerable time was provided for the stacking of COF nanosheets in the solvent evaporation process; thus, horizontally stacked COF layers were thermodynamically favorable in this case. Additionally, energy-dispersive X-ray spectroscopy (EDX) confirmed the uniform distribution of C, N, and O elements (Supporting Information, Figure S38), suggesting the homogeneity of the COF films. Such a morphology makes a sharp contrast to the agglomeration in COF powders, and the hierarchical porosity could facilitate the mass transport within the films. Therefore, our method provides a new aspect for synthesizing crystalline COF films with a controlled morphology toward plenty of applications, such as ion conductors,²³ supercapacitors,²⁴ and batteries,²¹ in which mass transport plays a key role.

Iodine Uptake with Accelerated Adsorption Kinetics. To demonstrate the utility of the COF films in the mass-transfer applications, we subjected these COF films to iodine adsorption. Nuclear fission generates a radioiodine pollutant, which is highly volatile and quickly disperses in the air and thus makes a serious threat to environmental and personal health.²⁵ COF powders and aerogels have been studied for the capture and storage of radiological iodine and have achieved a high iodine uptake of over 10 g g⁻¹.²⁶ However, they usually require

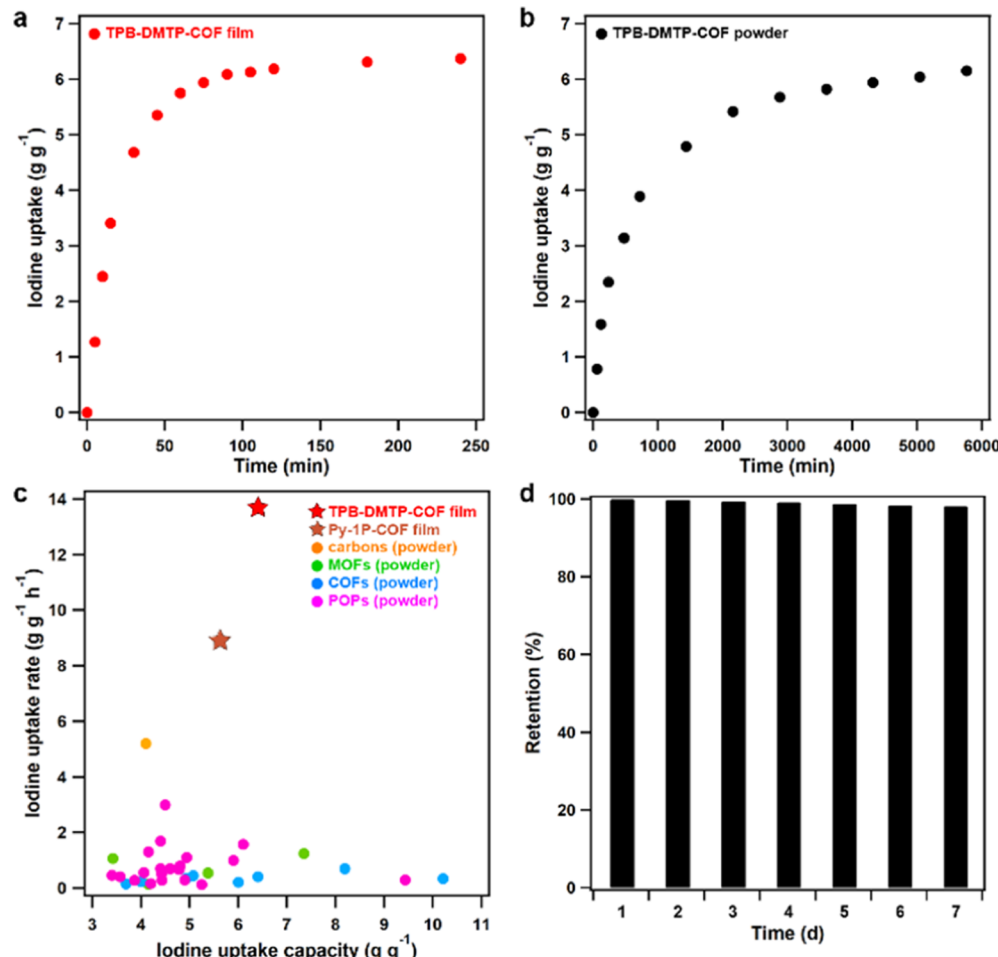


Figure 4. (a) Iodine uptake of the TPB-DMTP-COF film as a function of exposure time at 350 K and ambient pressure. (b) Iodine uptake of the TPB-DMTP-COF powder as a function of exposure time at 350 K and ambient pressure. (c) Iodine uptake capacities and rates of different adsorbents. The red and brown stars represent the COF films in this work, and the orange, green, sky-blue, and magenta cycles correspond to other previously reported adsorbents. (d) Iodine retention of the iodine-captured TPB-DMTP-COF film upon exposure to air at 25 °C and ambient pressure.

dozens of hours to reach an adsorption equilibrium. Such slow kinetics results from the slow diffusion of iodine in the long one-dimensional (1D) channels in the COF powders and aerogels; the slow adsorption kinetics lead to a substantial issue for practical utilization. We investigated iodine vapor capture by exposing the COF films to iodine vapor at 350 K under ambient pressure. TPB-DMTP-COF films exhibited exceptionally rapid adsorption, yielding a steep increment over 30 min and then saturating within 240 min to reach an uptake capacity of 6.37 g g⁻¹ (Figure 4a). This high adsorption rate made a sharp contrast to that of TPB-DMTP-COF powder, which increased over 36 h and saturated within 96 h to yield a similar uptake capacity of 6.15 g g⁻¹ (Figure 4b). Similarly, the TRITER-1-COF and Py-1P-COF films exhibited rapid uptake with the capacities of 1.47 and 5.58 g g⁻¹, respectively, within a short period of 240 min (Supporting Information, Figures S39 and S40). We calculated the rate constants using the time-dependent adsorption curves at their initial stages (unsaturated region). The rate constants of the COF films were 13.69, 3.06, and 8.93 g g⁻¹ h⁻¹ for TPB-DMTP-COF, TRITER-1-COF, and Py-1P-COF, respectively, which were 2.6 to 100 times higher than those of the state-of-the-art iodine adsorbents, including carbons, metal–organic frameworks (MOFs), COFs, and amorphous porous organic polymers (POPs) (Figure 4c).

Supporting Information, Table S4). Even though some porous materials showed a high iodine uptake capacity of over 7 g g⁻¹, such materials were difficult to be practically applied because of their torpid adsorption kinetics. By contrast, the high uptake kinetics in our COF films is attributed to the synergistic effect from the hierarchical porosity and reduced particle size that facilitates the diffusion of iodine in the short 1D channels. This is a clear demonstration of promoting mass transport in the COF films.

Notably, under ambient conditions (25 °C and 1 bar), the iodine-captured COF films can hold iodine without iodine escape even upon exposure to air (Figure 4d, Supporting Information, Figure S41). The iodine-captured COF films were recyclable for five cycles upon methanol rinse (Supporting Information, Figure S42) while retaining their chemical structures, crystallinities, and porosities, as evident by their IR spectra, PXRD profiles, and N₂-sorption isotherms (Supporting Information, Figures S43–S45). The superior adsorption kinetics and high uptake capacity combined with the structural robustness of the COF films render them a highly promising platform for iodine adsorption and other mass-transport-related applications.

In summary, we have described an unprecedented strategy of electrocleavage synthesis that is general and adaptable to

synthesize most imine-linked 2D COF films, with a synthetically controlled chemical structure and crystallinity. This method involves two key steps: cathodic reduction and protonation that exfoliates COF powders to nanosheets and anodic oxidation to recover the imine-linked crystalline COF films. The COF films are crucial to be utilized in many mass-transport-related applications, as demonstrated by the exceptional iodine uptake with superior kinetics. We believe that by structure screening and control over the electrochemical conditions, such an electrocleavage strategy could be utilized to synthesize other kinds of linkages, such as C=C bonds-, ketoneamine-, and triazine-linked COFs, thus being developed into a general method for high-quality COF film synthesis in the near future. Given the structural diversity and flexibility of COFs, we anticipate the emergence of an exciting field in designing COF films, which would significantly expand the potential of COFs for applications.

ASSOCIATED CONTENT

Supporting Information

The Supporting Information is available free of charge at <https://pubs.acs.org/doi/10.1021/jacs.1c13072>.

Synthetic procedures, FT-IR, PXRD, electrochemistry, UV-vis spectra, gas adsorption, TEM, SEM, iodine sorption, and stability test ([PDF](#))

AUTHOR INFORMATION

Corresponding Authors

Cheng Gu – State Key Laboratory of Luminescent Materials and Devices, Institute of Polymer Optoelectronic Materials and Devices and Guangdong Provincial Key Laboratory of Luminescence from Molecular Aggregates, South China University of Technology, Guangzhou 510640, P. R. China; [orcid.org/0000-0001-5259-6203](#); Email: gucheng@scut.edu.cn

Yuguang Ma – State Key Laboratory of Luminescent Materials and Devices, Institute of Polymer Optoelectronic Materials and Devices and Guangdong Provincial Key Laboratory of Luminescence from Molecular Aggregates, South China University of Technology, Guangzhou 510640, P. R. China; [orcid.org/0000-0003-0373-5873](#); Email: ygma@scut.edu.cn

Authors

Lingling Wang – State Key Laboratory of Luminescent Materials and Devices, Institute of Polymer Optoelectronic Materials and Devices, South China University of Technology, Guangzhou 510640, P. R. China; Science Center for Material Creation and Energy Conversion, Institute of Frontier and Interdisciplinary Science, Shandong University, Qingdao 266237, P. R. China

Changwen Xu – State Key Laboratory of Luminescent Materials and Devices, Institute of Polymer Optoelectronic Materials and Devices, South China University of Technology, Guangzhou 510640, P. R. China

Weiqi Zhang – State Key Laboratory of Luminescent Materials and Devices, Institute of Polymer Optoelectronic Materials and Devices, South China University of Technology, Guangzhou 510640, P. R. China; [orcid.org/0000-0002-8487-4949](#)

Qinglei Zhang – State Key Laboratory of Luminescent Materials and Devices, Institute of Polymer Optoelectronic

Materials and Devices, South China University of Technology, Guangzhou 510640, P. R. China

Manlin Zhao – State Key Laboratory of Luminescent Materials and Devices, Institute of Polymer Optoelectronic Materials and Devices, South China University of Technology, Guangzhou 510640, P. R. China

Cheng Zeng – State Key Laboratory of Luminescent Materials and Devices, Institute of Polymer Optoelectronic Materials and Devices, South China University of Technology, Guangzhou 510640, P. R. China

Qinglin Jiang – State Key Laboratory of Luminescent Materials and Devices, Institute of Polymer Optoelectronic Materials and Devices, South China University of Technology, Guangzhou 510640, P. R. China

Complete contact information is available at:
<https://pubs.acs.org/10.1021/jacs.1c13072>

Author Contributions

L.W. and C.X. contributed equally.

Notes

The authors declare no competing financial interest.

ACKNOWLEDGMENTS

This work was supported by the National Natural Science Foundation of China (21975078), the Guangdong Basic and Applied Basic Research Foundation (2021A1515010311), the Natural Science Foundation of Guangdong Province (2019B030301003), the 111 Project (BP0618009), and the Thousand Youth Talents Plan. C.G. acknowledges the scholarship support from the China Scholarship Council (202006155049).

REFERENCES

- (1) Côté, A. P.; Benin, A. I.; Ockwig, N. W.; O'Keffe, M.; Matzger, A. J.; Yaghi, O. M. Porous, Crystalline, Covalent Organic Frameworks. *Science* **2005**, *310*, 1166.
- (2) Li, Y.; Chen, W.; Xing, G.; Jiang, D.; Chen, L. New Synthetic Strategies toward Covalent Organic Frameworks. *Chem. Soc. Rev.* **2020**, *49*, 2852.
- (3) Su, Y.; Wan, Y.; Xu, H.; Otake, K.-i.; Tang, X.; Huang, L.; Kitagawa, S.; Gu, C. Crystalline and stable benzofuran-linked covalent organic frameworks from irreversible cascade reactions. *J. Am. Chem. Soc.* **2020**, *142*, 13316.
- (4) Wang, Z.; Zhang, S.; Chen, Y.; Zhang, Z.; Ma, S. Covalent Organic Frameworks for Separation Applications. *Chem. Soc. Rev.* **2020**, *49*, 708.
- (5) Zhang, H.; Gu, C.; Yao, M. S.; Kitagawa, S. Hybridization of Emerging Crystalline Porous Materials: Synthesis Dimensionality and Electrochemical Energy Storage Application. *Adv. Energy Mater.* **2021**, *12*, 2100321.
- (6) Han, X.; Xia, Q.; Huang, J.; Liu, Y.; Tan, C.; Cui, Y. Chiral Covalent Organic Frameworks with High Chemical Stability for Heterogeneous Asymmetric Catalysis. *J. Am. Chem. Soc.* **2017**, *139*, 8693.
- (7) Li, J.; Jing, X.; Li, Q.; Li, S.; Gao, X.; Feng, X.; Wang, B. Bulk COFs and COF Nanosheets for Electrochemical Energy Storage and Conversion. *Chem. Soc. Rev.* **2020**, *49*, 3565.
- (8) Zhao, S.; Jiang, C.; Fan, J.; Hong, S.; Mei, P.; Yao, R.; Liu, Y.; Zhang, S.; Li, H.; Zhang, H.; Sun, C.; Guo, Z.; Shao, P.; Zhu, Y.; Zhang, J.; Guo, L.; Ma, Y.; Zhang, J.; Feng, X.; Wang, F.; Wu, H.; Wang, B. Hydrophilicity Gradient in Covalent Organic Frameworks for Membrane Distillation. *Nat. Mater.* **2021**, *20*, 1551.
- (9) Kong, Y.; He, X.; Wu, H.; Yang, Y.; Cao, L.; Li, R.; Shi, B.; He, G.; Liu, Y.; Peng, Q.; Fan, C.; Zhang, Z.; Jiang, Z. Tight Covalent Organic Framework Membranes for Efficient Anion Transport via

- Molecular Precursor Engineering. *Angew. Chem., Int. Ed.* **2021**, *60*, 17638.
- (10) Liu, K.; Qi, H.; Dong, R.; Shihhare, R.; Addicoat, M.; Zhang, T.; Sahabudeen, H.; Heine, T.; Mannsfeld, S.; Kaiser, U.; Zheng, Z.; Feng, X. On-Water Surface Synthesis of Crystalline, Few-Layer Two-Dimensional Polymers Assisted by Surfactant Monolayers. *Nat. Chem.* **2019**, *11*, 994.
- (11) Hao, Q.; Zhao, C.; Sun, B.; Lu, C.; Liu, J.; Liu, M.; Wan, L.-J.; Wang, D. Confined Synthesis of Two-Dimensional Covalent Organic Framework Thin Films within Superspreading Water Layer. *J. Am. Chem. Soc.* **2018**, *140*, 12152.
- (12) Chandra, S.; Kandambeth, S.; Biswal, B. P.; Lukose, B.; Kunjir, S. M.; Chaudhary, M.; Babarao, R.; Heine, T.; Banerjee, R. Chemically Stable Multilayered Covalent Organic Nanosheets from Covalent Organic Frameworks via Mechanical Delamination. *J. Am. Chem. Soc.* **2013**, *135*, 17853.
- (13) Khayum, M. A.; Kandambeth, S.; Mitra, S.; Nair, S. B.; Das, A.; Nagane, S. S.; Mukherjee, R.; Banerjee, R. Chemically Delaminated Free-Standing Ultrathin Covalent Organic Nanosheets. *Angew. Chem., Int. Ed.* **2016**, *55*, 15604.
- (14) Mitra, S.; Kandambeth, S.; Biswal, B. P.; Khayum, M. A.; Choudhury, C. K.; Mehta, M.; Kaur, G.; Banerjee, S.; Prabhune, A.; Verma, S.; Roy, S.; Kharul, U. K.; Banerjee, R. Self-Exfoliated Guanidinium-Based Ionic Covalent Organic Nanosheets (iCONs). *J. Am. Chem. Soc.* **2016**, *138*, 2823.
- (15) Wang, L.; Zeng, C.; Xu, H.; Yin, P.; Chen, D.; Deng, J.; Li, M.; Zheng, N.; Gu, C.; Ma, Y. A Highly Soluble, Crystalline Covalent Organic Framework Compatible with Device Implementation. *Chem. Sci.* **2019**, *10*, 1023.
- (16) Yan, M.; Kawamata, Y.; Baran, P. S. Synthetic Organic Electrochemical Methods Since 2000: On the Verge of a Renaissance. *Chem. Rev.* **2017**, *117*, 13230.
- (17) Wang, P.; Xu, Q.; Li, Z.; Jiang, W.; Jiang, Q.; Jiang, D. Exceptional Iodine Capture in 2D Covalent Organic Frameworks. *Adv. Mater.* **2018**, *30*, 1801991.
- (18) Gomes, R.; Bhanja, P.; Bhattacharjee, A. A Triazine-based Covalent Organic Polymer for Efficient CO₂ Adsorption. *Chem. Commun.* **2015**, *51*, 10050.
- (19) Ascherl, L.; Evans, E. W.; Hennemann, M.; Di Nuzzo, D.; Hufnagel, A. G.; Beetz, M.; Friend, R. H.; Clark, T.; Bein, T.; Auras, F. Solvatochromic Covalent Organic Frameworks. *Nat. Commun.* **2018**, *9*, 3802.
- (20) Wang, L.-L.; Jiang, Q.-L.; Zhao, D.-K.; Zhang, Q.-L.; Jia, Y.-H.; Gu, C.; Hu, D.-H.; Ma, Y.-G. Triazine and Porphyrin-Based Cross-Linked Conjugated Polymers: Protonation-Assisted Dissolution and Thermoelectric Properties. *CCS Chem.* **2020**, *3*, 2688.
- (21) Wang, S.; Wang, Q.; Shao, P.; Han, Y.; Gao, X.; Ma, L.; Yuan, S.; Ma, X.; Zhou, J.; Feng, X.; Wang, B. Exfoliation of Covalent Organic Frameworks into Few-Layer Redox Active Nanosheets as Cathode Materials for Lithium-Ion Batteries. *J. Am. Chem. Soc.* **2017**, *139*, 4258.
- (22) Ferriante, C.; Evans, A. M.; Jhulki, S.; Castano, I.; Strauss, M. J.; Barlow, S.; Dichtel, W. R.; Marder, S. R. New Mechanistic Insights into the Formation of Imine-Linked Two-Dimensional Covalent Organic Frameworks. *J. Am. Chem. Soc.* **2020**, *142*, 18637.
- (23) Zhang, G.; Hong, Y.-I.; Nishiyama, Y.; Bai, S.; Kitagawa, S.; Horike, S. Accumulation of Glassy Poly(ethylene oxide) Anchored in a Covalent Organic Framework as a Solid-State Li⁺ Electrolyte. *J. Am. Chem. Soc.* **2019**, *141*, 1227.
- (24) Zhang, H.; Tang, X.; Zhao, D.; Zheng, N.; Huang, L.; Sun, T.; Gu, C.; Ma, Y. Suppressing Charge Trapping Effect in Ambipolar Conducting Polymer with Vertically Standing Graphene as the Composite Electrode for High Performance Supercapacitor. *Energy Storage Mater.* **2020**, *29*, 281.
- (25) Mushkacheva, G.; Rabinovich, E.; Privalov, V.; Povolotskaya, S.; Shorokhova, V.; Sokolova, S.; Turdakova, V.; Ryzhova, E.; Hall, P.; Schneider, A. B.; Preston, D. L.; Ron, E. Thyroid Abnormalities Associated with Protracted Childhood Exposure to ¹³¹I from

Atmospheric Emissions from the Mayak Weapons Facility in Russia. *Radiat. Res.* **2006**, *166*, 715.

(26) Xie, Y.; Pan, T.; Lei, Q.; Chen, C.; Dong, X.; Yuan, Y.; Shen, J.; Cai, Y.; Zhou, C.; Pinnau, I.; Han, Y. Ionic Functionalization of Multivariate Covalent Organic Frameworks to Achieve an Exceptionally High Iodine-Capture Capacity. *Angew. Chem., Int. Ed.* **2021**, *60*, 22432.

□ Recommended by ACS

Structural and Electronic Modulations of Imidazolium Covalent Organic Framework-Derived Electrocatalysts for Oxygen Redox Reactions in Rechargeable Zn–Air ...

Jong-Min Ju, Jong-Ho Kim, et al.

MAY 18, 2022

ACS APPLIED MATERIALS & INTERFACES

READ ▶

Industrial-Current-Density CO₂-to-C2+ Electroreduction by Anti-swelling Anion-Exchange Ionomer-Modified Oxide-Derived Cu Nanosheets

Yuan Zhao, Yi Xie, et al.

MAY 31, 2022

JOURNAL OF THE AMERICAN CHEMICAL SOCIETY

READ ▶

Constructing Stable Chromenoquinoline-Based Covalent Organic Frameworks via Intramolecular Povarov Reaction

Xiao-Rui Ren, Dong Wang, et al.

FEBRUARY 07, 2022

JOURNAL OF THE AMERICAN CHEMICAL SOCIETY

READ ▶

Microchemical Engineering in a 3D Ordered Channel Enhances Electrocatalysis

Qing-Xia Chen, Shu-Hong Yu, et al.

JULY 21, 2021

JOURNAL OF THE AMERICAN CHEMICAL SOCIETY

READ ▶

Get More Suggestions >